Hydrothermal synthesis of homogenous and size-controlled uranium-thorium oxide micro-particles for nuclear safeguards

P. Asplanato, W. Zannouh, A.L. Fauré, P.H. Imbert, J. Lautru, M. Cornaton, N. Dacheux, F. Pointurier, Nicolas Clavier

Hydrothermal synthesis of homogenous and size-controlled uranium-thorium oxide micro-particles for nuclear safeguards

P. Asplanato [1,2], W. Zannouh [2], A.L. Fauré [1], P.H. Imbert [2], J. Lautru [2], M. Cornaton [1], N. Dacheux [2], F. Pointurier [1], N. Clavier [2,*]

[1] *CEA, DAM, DIF, 91297 Arpajon, France*

[2] *ICSM, Univ Montpellier, CEA, CNRS, ENSCM, Marcoule, France*

* Corresponding author:

Dr. Nicolas CLAVIER
ICSM, Univ Montpellier, CEA, CNRS, ENSCM
Site de Marcoule
BP 17171
30207 Bagnols sur Cèze
France

Phone : + 33 4 66 33 92 08
Fax : + 33 4 66 79 76 11

nicolas.clavier@icsm.fr

Abstract :

Particle analysis is one of the key-techniques used in the field of nuclear safeguards. Beyond traditional uranium isotopic ratio measurement, other methodologies are implemented to better characterize nuclear materials. Among them, age dating at the particle scale enables to determine the time elapsed since the last chemical step of separation/purification or enrichment. The ^{230}Th-^{234}U couple being one of the most common radiochronometer, there is a need for morphology and size controlled uranium-thorium mixed oxides particles that could be used as reference materials during isotopic measurements. With this aim, uranium-thorium mixed oxide microspheres were synthesized using a wet chemistry route. The hydrothermal conversion of aspartate precursors at T = 433 K led to mixed dioxide micro-particles with controlled spherical morphology and size, up to 5 mol.% in thorium. In order to remove impurities, densify the micro-particles, and control the chemical form of the final compounds, heat treatments were performed under various atmospheres. Nearly stoichiometric (U,Th)O_2 dioxides were obtained under reducing conditions (Ar-4%H_2) while U_3O_8-based samples were formed under air, with thorium incorporated in the structure up to 2 mol.%. Last, the homogeneity of the cation distributions in the samples was evaluated by various methods, including PERALS α-scintillation counting, as well as X-EDS and LG-SIMS analyses of individual particles, leading to consistent results. Particularly, the relative external reproducibility (2σ) of the $^{232}Th^+/^{238}U^+$ ion ratios measured at the particle scale remained below 10%, paving the way to use these mixed oxide particles in the field of nuclear safeguards.

Keywords :

Uranium oxide – thorium oxide – hydrothermal synthesis – morphology control – nuclear safeguards

Introduction

Particle analysis is one of the key-techniques used in the field of nuclear safeguards, especially to ensure the respect of the treaty of non-proliferation of nuclear weapons (NPT). In this frame, inspectors from the International Atomic Energy Agency collect dust samples in nuclear facilities worldwide by rubbing surfaces with cotton wipers [1, 2]. The samples collected on-site generally contain only tens to a few hundreds of particles of interest, i.e. coming from and representative of the nuclear materials held in the inspected facilities. Moreover, they are frequently sub-micrometric in size, which make their analyses challenging. The actinide-bearing particles are generally analyzed by mass spectrometry techniques (Secondary Ion Mass Spectrometry - SIMS, Thermo-Ionization Mass Spectrometry - TIMS) by a handful of highly specialized laboratories in order to determine actinide isotopic ratios that can inform on the use of the fissile matter (e.g. $^{235}U/^{238}U$). Other isotopic ratios can be used as radiochronometer to determine the « age » of the material, i.e. the time spent since the last chemical step of separation/purification or enrichment [3-7]. Indeed, during their production, nuclear fuels endure several processes of chemical purification, consisting of impurities elimination, including that of radioactive decay products. In the hypothesis of a complete separation, the elapsed time since the last purification can be calculated thanks to the parent-daughter ratio in the samples [8]. In the case of uranium, the most common radiochronometer is ^{230}Th-^{234}U. The "age" t of the U-bearing material is linked to the $^{230}Th/^{234}U$ ratio thanks to the following relation:

$$t = \frac{1}{\lambda_U - \lambda_{Th}} \times ln\left(1 - \frac{N_{Th}^t}{N_U^t} \times \frac{\lambda_{Th} - \lambda_U}{\lambda_U}\right) \qquad (1.)$$

where λ_U and λ_{Th} are the activity constants of ^{234}U and ^{230}Th, respectively, and N^t_U and N^t_{Th}, are the numbers of atoms of ^{234}U and ^{230}Th at a given time t [9]. In this expression, assumption is made that head radionuclide, i.e. ^{234}U, is not significantly decaying during the elapsed time, hence that its number of atom can be considered constant compared to the starting content.

The "age" of fissile materials, combined with the knowledge of the uranium isotopic composition, is a very important information for nuclear safeguards. Hence, a few laboratories involved in particle analysis have attempted to develop analytical procedures to carry out age-determination at the particle scale by means of SIMS [10, 11]. However, these analyses suffer from the lack of reference materials for validating the methods and evaluating their performance, although uranium oxide micro-particles were recently certified in this aim [12]. Another key-point is the determination of the U-Th fractionation factor, which may be time and matrix-dependent. Currently highly enriched uranium particles from certified reference materials of known production date are used [10, 11]. Beyond the risk of contamination and memory effect inside the instrument, such particles are not available for all laboratories. In

order to improve the accuracy of the analytical methods employed, and to open the possibility to have reference samples of controlled size, morphology and chemical/isotopic composition, it is of great importance to investigate the fabrication of uranium-thorium oxide micro particles.

Although of great interest for various applications, the synthesis of size and morphology-controlled mixed uranium-thorium oxide particles has been rarely discussed in the literature. Conversely, some works focused on either ThO_2 or UO_2/U_3O_8 samples, or on surrogate oxides such as CeO_2, but addressed very different scales. For example, the impregnation of resin beads with a solution containing actinides, followed by a heat treatment at high temperature, led to the preparation of sub-millimetric spherical oxide particles [13]. Quite similarly, the use of sol-gel processes allowed to synthesize uranium oxide microspheres with a diameter in the 100 – 500 µm range [14, 15]. At the other end of the size scale, Hudry *et al.* synthesized actinide oxide nanoparticles, including UO_2 and ThO_2, through the solvothermal decomposition of mixture containing thorium acetylacetonate or uranyl acetate together with oleic acid, tri-n-octylamine, tri-n-octylphosphine oxide and benzyl ether [16]. Beyond wet chemistry routes, alternative methods based on pyrolysis techniques were also tested. Particularly, the IEK-6 group at FZ Julich (Germany) has developed for several years the synthesis of U_3O_8 micro particles (potentially doped with Nd^{3+}) with a size of around 1 µm in diameter, mechanically controlled from the diameter of the droplets formed in the aerosol by vibrating orifices [17-20].

More recently, several authors explored hydrothermal methods to provide easy, rapid and versatile routes for the synthesis of actinides oxide micro-particles. The protocols are usually based on the initial complexation of actinide cations by an organic ligand followed by the hydrothermal decomposition of this latter and the hydrolysis of the cation. For example, Nkou Bouala *et al.* obtained UO_2 nanospheres thanks to the complexation of U^{4+} with polyethylene glycol [21], while micro-particles of UO_{2+x} were obtained under certain conditions of pH by Manaud *et al.* during the hydrothermal conversion of U(IV) oxalates [22]. In the case of Th-based compounds, several authors reported the preparation of size-controlled ThO_2 spherical particles by tuning the initial molar ratios in Th/organics mixtures, involving for example sodium dodecyl sulfate ($C_{12}H_{25}O_4SNa$) or hexamethylene tetramine ($C_6H_{12}N_4$) [23, 24].

With the aim to provide a robust protocol for the synthesis of uranium-thorium oxide micro particles for nuclear safeguards, we report herein a simple and direct method based on the hydrothermal conversion of aspartate precursors. The raw particles obtained from the hydrothermal process were first characterized from the structural (PXRD) and morphological point of view (SEM), then calcined in various atmospheres to monitor the final stoichiometry of the oxide micro-particles and eliminate residual volatiles coming from the wet chemistry synthesis process. The behavior of the particles during the heat treatment was studied by TGA and HT-ESEM observations, before extensive characterization of the final product. In this frame, a particular attention was paid to the determination of the Th-content in the particles, and of the homogeneity of the thorium distribution at the macro- and micro-scales, as well as between individual particles. In this aim, different techniques were used to probe the chemical

composition, including α-scintillation spectrometry (Photo-Electron Rejecting Alpha Liquid Scintillation - PERALS), SEM-EDS and Large-Geometry – SIMS (LG-SIMS).

I. Experimental

I.1. Micro-particles synthesis

All the reagents used in this study were of analytical-grade and supplied by Sigma-Aldrich except uranium and thorium sources. On the one hand, the uranium source was prepared under the form of a U(IV) solution in hydrochloric media through the dissolution of uranium metal chips (kindly supplied by CETAMA, Marcoule, France). The metal pieces were first rinsed with dichloromethane, acetone and water, washed in 2M HCl in order to eliminate possible traces of uranium oxide present at the surface, and finally dissolved in 6M HCl. The high chloride concentration allows the stabilization of the tetravalent oxidation state of uranium in solution for several months [25]. The uranium concentration of the final solution was estimated to 0.620 ± 0.004 M by ICP-AES measurements. On the other hand, thorium chloride solution was obtained by dissolving thorium nitrate salt (supplied by Ibilabs) in concentrated 4 M HCl. The initial solution was repetitively evaporated then the residue dissolved in hydrochloric acid in order to remove residual traces of nitrate ions in solution. The thorium concentration in the final solution was estimated to 0.170 ± 0.002 M.

The protocol used for the synthesis of size-controlled uranium-thorium oxide spherical micro particles, with $0.005 \leq Th/(U+Th) \leq 0.300$ mole ratios, was adapted from Trillaud et al. [26], and based on the complexation of tetravalent uranium and thorium with aspartic acid, and further conversion of aspartate precursor into oxide under mild hydrothermal conditions. The first step consisted in dissolving 200 mg of L-aspartic acid in 10 mL of deionized H_2O (18.2 MΩ.cm at 298 K), acidified by the addition of 2-3 drops 6M HCl. Then, the hydrochloric solutions containing U^{4+} and Th^{4+} were mixed together with the desired molar ratio in order to reach a cation amount close to $5x10^{-4}$ mol. The obtained solution was further added dropwise to the aspartic acid, while maintaining continuously the pH close to 2 by adding ammonia or HCl. Once the mixture was complete, the solution was moved into a Teflon-lined autoclave (Parr, model #4749) and hydrothermal treatment was performed at 433 K during 30 hours. It is important to note that the solution was stirred during all the hydrothermal treatment by a magnetic agitator (2Mag-MixControl 20). During this study, we decided to fix the stirring speed at 950 rpm, which corresponds to a Reynold's number close to 12000. Based on the previous works on the uranium system, one could expect a particle diameter close to 1600-1700 nm [26]. After hydrothermal treatment, the autoclave was cooled down overnight before collecting the solid phase by centrifugation. In the same time, analysis of the supernatant showed only residual traces of uranium and thorium, evidencing the quantitative precipitation of the cations (precipitation yield systematically above 99.8 %).

The precipitate was further washed twice with deionized water and once with ethanol, and dried in an oven at 363 K for 6 hours. After synthesis, raw micro-particles were finally

calcined to remove residual organics and water, eliminate porosity and to tune the O/M stoichiometry. The heat treatments were performed under air or Ar-H_2 4% atmosphere, to reach either Th-doped U_3O_8 or UO_2, respectively. With this aim, samples were heated at 973 K with a rate of 3K.min^{-1}, temperature was held during 4 hours, then the samples were cooled down to room temperature at 3K.min^{-1}.

I.2. Samples characterization

PXRD: Powder X-Ray Diffraction (PXRD) diagrams were acquired by the means of a Bruker D8 diffractometer equipped with a Lynx-eye detector adopting the reflection geometry and using Cu$K\alpha_{1,2}$ radiation (λ = 1.54184 A°). PXRD patterns were recorded at room temperature in the 5° ≤ 2θ ≤ 100° range, with a step size of Δ(2θ) = 0.01 ° and a total counting time of about 3 hours per sample. To avoid any radioactive contamination, the powder was placed in a special sample holder (dome-shaped container with anti-scattering blade) that could generate additional large diffusion peak between 10 ° and 20 ° (2θ).

Structural analysis was processed by the Rietveld method using the Fullprof Suite Program [27]. All the refinements were performed using the Thompson-Cox-Hastings pseudo-Voigt profile convoluted with axial divergence asymmetry function [28]. The refined parameters were as follows: zero shift, unit cell parameters, scale factor, thermal displacement, background, and peak asymmetry. The microstructural parameters were obtained using an anisotropic size model.

ESEM: Before observation, the powdered samples were systematically dispersed in ethanol and deposited on a mirror-grade polished aluminum plate. Environmental Scanning Electron Microscope (ESEM) images were then directly recorded from the as-deposited powders without any additional preparation such as metallization. A FEI Quanta 200 scanning electron microscope, equipped with an Everhart-Thorley Detector (ETD) and a Back-Scattered Electron Detector (BSED) was used to record images with an acceleration voltage of 2 kV under high vacuum conditions. The average diameter of the micro-particles was determined by ImageJ software [29] and Feret method. Images were recorded with a x 5000 magnification with the aim to analyze at least 900 particles to reach good statistics.

The morphological evolution of the micro-particles during heat treatment at high temperature was also monitored *in situ* using a specific high temperature stage attached to the ESEM. The samples were heated from room temperature to 1273 K with a 5K.min^{-1} heating rate, while continuously recording high magnification images on selected grains. The gas pressure in the ESEM chamber was kept to 100 Pa during the experiment, either when using air or N_2-H_2 5%. Image processing to extract the grain diameter was performed using the ImageJ software.

TGA: Thermogravimetric analyses were undertaken thanks to a Setaram Setsys Evolution equipped either with a type-S thermocouple (Pt / Pt-10%Rh) when working in air or with a W5 device (W-5%Re / W-26%Re) for analyses performed under reducing atmosphere. After recording of a baseline using an empty crucible (100 µL), weight loss was monitored during a heat treatment up to 1273K with a heating rate of $5K.min^{-1}$.

Characterization of chemical composition and cationic homogeneity: In this study, three different yet complementary methods were used to determine both the chemical composition of the micro-particle samples (i.e. the amount of thorium incorporated), and the homogeneity of the uranium/thorium distribution.

First, full dissolution followed by PERALS (Photo-Electron Rejecting Alpha Liquid Scintillation) measurements allowed to assess the global composition of the samples. The complete dissolution of 10 mg of uranium-thorium oxide micro-particles was performed in 20 mL of 6M HCl at T = 333 K. Liquid/liquid extraction was achieved by contacting 1.5 mL of ALPHAEX^{TM} with 6 mL of aqueous phase in 10 mL Pyrex tubes. 1 mL of organic phase was further up-taken after centrifugation at 4500 rpm during 10 minutes. In a first step, the pH of the solution was fixed between 0 and 1 to extract only uranium [21]. In a second step, the pH of the solution was increased to 3 in order to extract both thorium and uranium. Thorium content was finally determined through the subtraction of the spectra obtained from the two fractions.

The homogeneity of the uranium/thorium distribution was then evaluated at the powder scale thanks to SEM-EDS analyses. The powders were first shaped as thin 5mm-diameter pellets by uniaxial pressing at about 200 MPa. This preliminary step was intended to guarantee a planar surface, perpendicular to the electron beam, thus allowing us to recover semi-quantitative data without losing the spherical shape of the particles. EDS analyses were carried out on about 100 individual particles. Although the analyzed volume by EDS ($\sim\mu m^3$) was roughly equivalent to the particles volume, the influence of adjacent particles may not be completely ruled out. The distribution of the Th/(U+Th) molar ratio was finally fitted by a Gaussian law, and the result expressed as the average value with a 95% confidence interval (2σ).

Last, LG-SIMS analyses were performed to determine precisely the ratios of the signal recorded for the $^{232}Th^+$ ions to the one recorded for the $^{238}U^+$ ions in individual particles. This measurement was repeated for 30 micro-particles, offering the possibility to evaluate the variability of the chemical composition from one micro-particle to another. The LG-SIMS measurements were performed with a CAMECA IMS 1300HR^3, equipped with a Hyperion II RF plasma oxygen source from Oregon Physics (Beaverton, OR, USA). Such a primary oxygen ion beam is typically used to enhance the production of electropositive ions such as U^+ and Th^+. All the analyses were done with a primary high voltage of +15 kV, a sample high voltage of + 8 kV, a mass resolution power around 4000 and a focused primary beam intensity of 70 pA, with no raster. The ionic species, $^{232}Th^+$ and $^{238}U^+$, were recorded in a single collection mode using a single electron multiplier.

II. Results

II.1. Characterization of as-precipitated particles

II.1.1. Structural characterization

The powders obtained directly after the hydrothermal conversion process were first analyzed by PXRD. The patterns collected for various Th-doping rates are gathered in **Figure 1**, and all present the characteristic PXRD lines of the fluorite-type structure adopted by both UO_2, ThO_2 and associated solid solutions. Nevertheless, the peaks were systematically found to be large and of low intensity. In this case, this feature is mainly associated to a small crystallite size, i.e. a short length of coherence domains, although the presence of an amorphous phase cannot be completely ruled out. This conclusion was made based on previous reports concerning the synthesis of actinide dioxides through the hydrothermal conversion of carboxylate precursors [22, 30, 31]. Indeed, the various authors systematically ended-up with nanostructured samples formed by the assembly of elementary crystallites of a few nanometers.

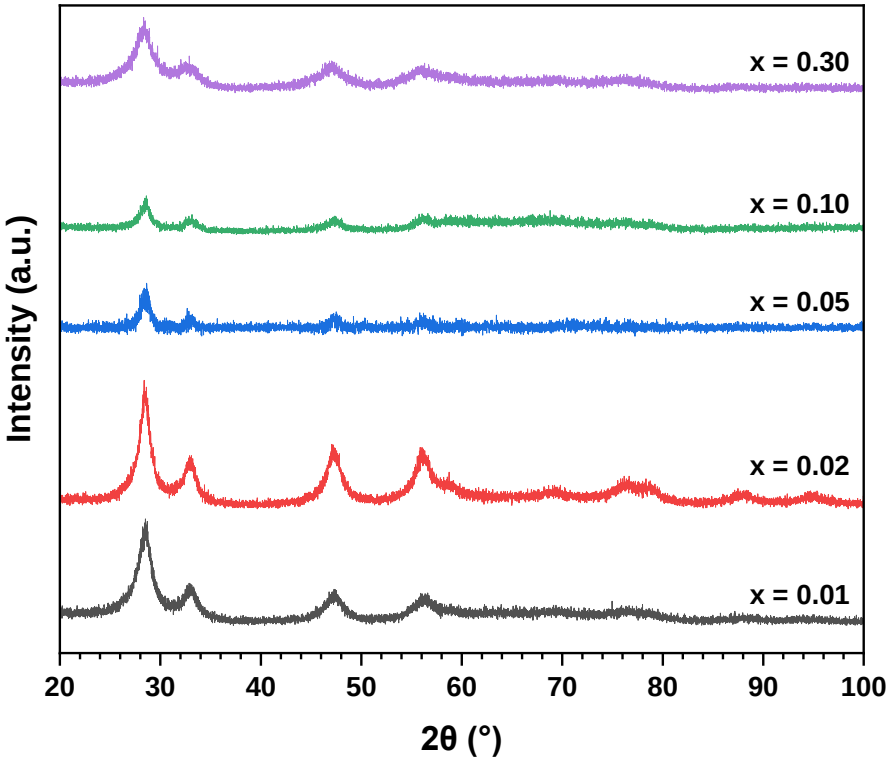

Figure 1. PXRD patterns collected for $U_{1-x}Th_xO_{2+\delta}.nH_2O$ uranium(IV)-thorium oxide particles obtained directly after the hydrothermal treatment of aspartate precursors.

In order to get further insights on the structural characteristics of the samples, Rietveld refinement was performed on the PXRD patterns, even if some of our data remained unusable due to the very low intensity of the diffractograms. As a result, **Table 1** reports the values obtained in terms of unit cell parameters and average crystallite sizes.

As expected from the general outline of the PXRD patterns, the average crystallite size was found to be very small, and typically ranged between 5 and 10 nm. Also, it seemed to decrease slightly when adding thorium in the sample. In parallel, the unit cell parameter was found to increase with thorium incorporation, in agreement with the ionic radii of both elements in the eight-fold coordination (i.e. 1.05 Å for Th^{4+} and 1.00 Å for U^{4+}) [32]. More importantly, the quasi-linear variation of the unit cell parameter versus the thorium incorporation rate (**Figure 2**) evidences the formation of a solid solution, rather than the precipitation of distinct oxides. On the basis of these results, and taking into account the fact that the formation of oxide phases during hydrothermal processes generally result from the aging of an hydroxide intermediate [33], we can propose the general formula of our samples to be written as $U_{1-x}Th_xO_{2+\delta}.nH_2O$, with a δ value that might evolve through time if no precautions are taken to prevent U(IV) from oxidation.

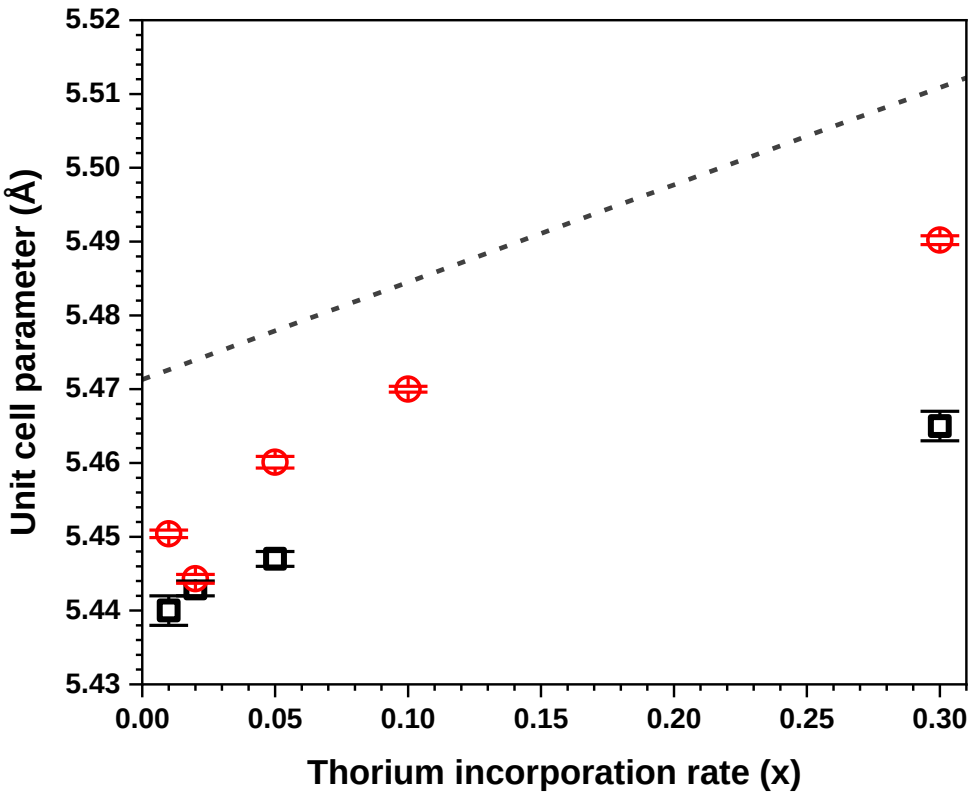

Figure 2. Variation of the unit cell parameter of the $U_{1-x}Th_xO_{2+\delta}.nH_2O$ micro-particles recovered from hydrothermal conversion process (□) and after heat treatment at 1273K under Ar-4%H_2 (○). The dotted line represents the Vegard's law between reference data reported in the literature for bulk UO_2 and ThO_2 [34, 35].

Table 1. Unit cell parameter and average crystallite sizes of the $U_{1-x}Th_xO_{2+\delta}.nH_2O$ samples recovered from hydrothermal conversion process.

x	**0.01**	**0.02**	**0.05**	**0.30**
a (Å)	5.440(2)	5.443(1)	5.447(1)	5.465(2)
Crystallite size (nm)	8	7	5	4

II.1.2. ESEM observations

The solid phases recovered from the hydrothermal treatment of the uranium (IV)-thorium aspartate precursors were then observed by ESEM in order to confirm the formation of morphology-controlled particles (**Figure 3**). As expected from the previous work by Trillaud *et al.* [26], the precipitates were systematically under the form of micro-particles presenting a spherical habit. However, strong modifications were noted when varying the thorium content. Up to x = 0.05, the microspheres appeared to be mainly monodisperse, with a diameter in the 1-2 µm range. Conversely, for compositions exceeding 5 mol.% in thorium, the particles collected were found to be significantly smaller, typically between 50 and 250 nm, and presented a larger variation in size. Although monodispersity is not the only acceptance criteria for standard particles in nuclear safeguards, these observations somehow limit the preparation of uranium-thorium reference materials to around 5 mol.% in thorium. However, this does not appear as a drawback, as the amount of ^{230}Th to be measured in real field-samples is expected to be very low. Indeed, it is typically around few attograms (*i.e.* 10^{-18} g) per particle, due to the young age of the samples that cannot exceed 70 years [9, 11], and would anyway reach only tenths to hundreds of attograms in natural uranium when reaching the secular equilibrium.

When monodisperse micrometric particles were obtained, image analysis was performed in order to get statistical information on the average diameter of the microspheres and its variation. In this aim, the Feret diameter of about 900 particles was determined using the ImageJ software [29]. As a matter of example, the size-distribution for the particles with x = 0.05 is plotted in **Figure 4**. Similar results were obtained for x = 0.005; 0.01 and 0.02. For all the samples studied, the Feret diameter distribution could be fitted with a Gaussian law. As such, the average diameter values reported in **Table 2** are expressed with a ± 2σ standard deviation, this range then comprising 95% of the particles in the sample. It is important to underline that this 2σ value does not represent in any case the accuracy of the measurement, or an uncertainty attached to the average value, but reflects the size variation from one single particle to another in the batch.

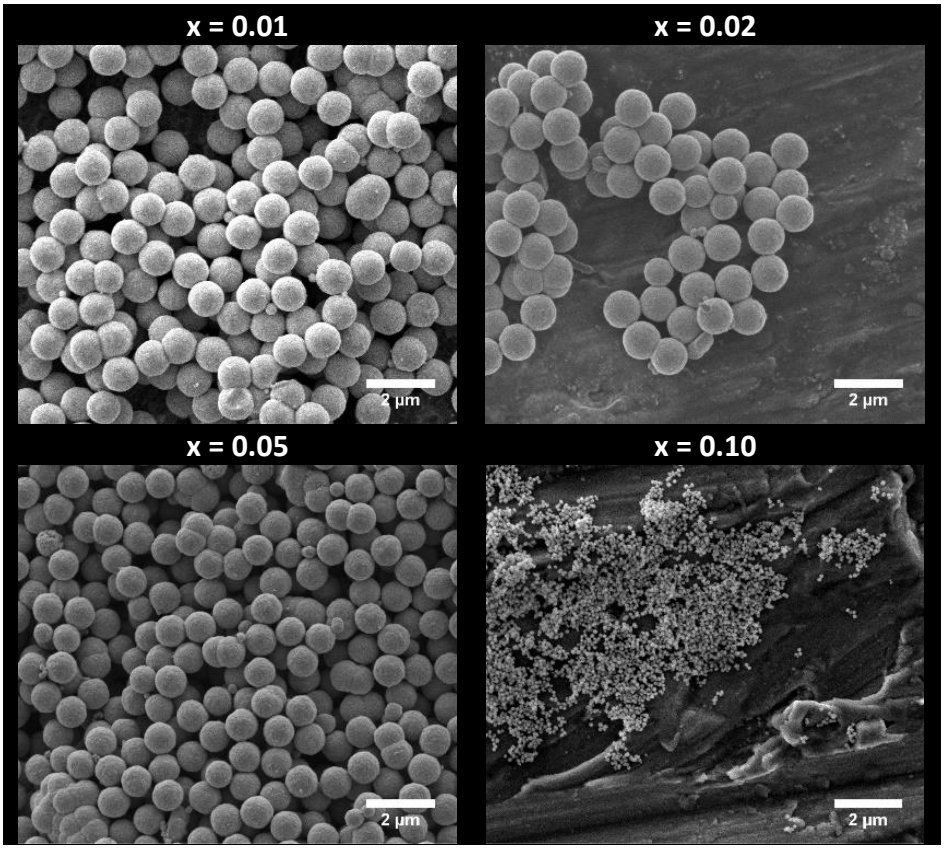

Figure 3. SEM observations of the $U_{1-x}Th_xO_{2+\delta}.nH_2O$ uranium-thorium oxide particles obtained directly after the hydrothermal treatment of aspartate precursors.

For all the compositions tested in the $0.05 \leq x \leq 0.5$ range, the average diameter of the micro-particles remained close to 1600-1700 nm. This value is similar to that determined previously for pure UO_2 particles, i.e. 1670 ± 210 nm [18]. Also, the size dispersion was systematically close to 10-15% of the average value, which remains in the same order of magnitude than that reported by Trillaud *et al.* [26], but evidences better size and shape control than in other chemical methods such as that described by Hudry *et al.* when preparing mixed uranium-thorium nanoparticles [36].

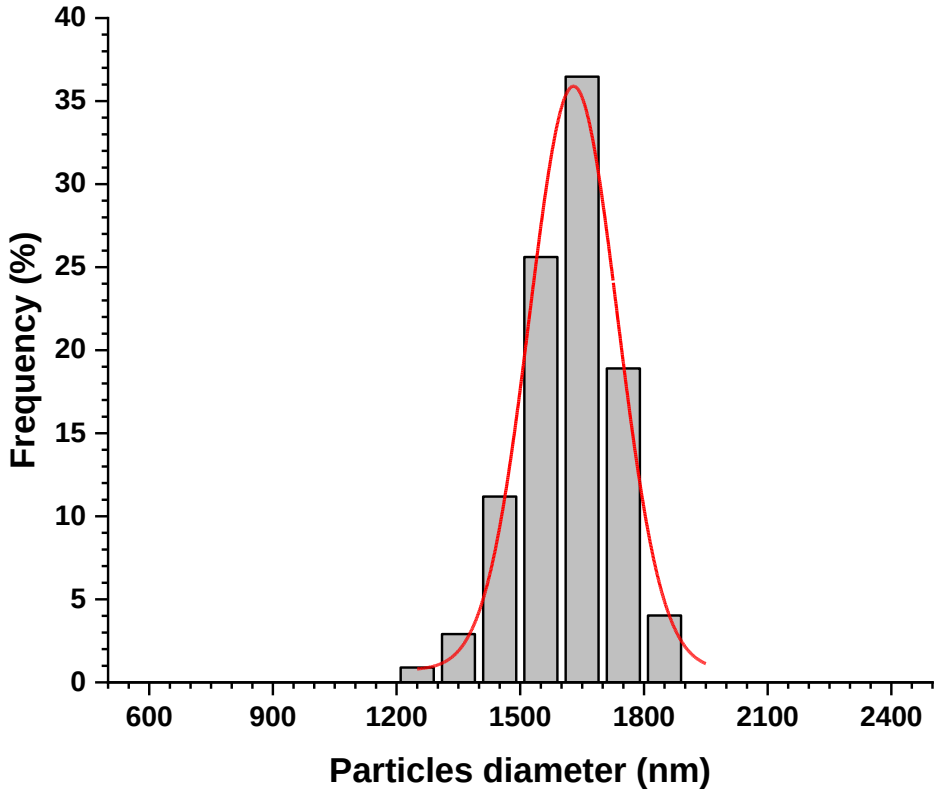

Figure 4. Statistical distribution of the Feret diameters of the particles for x = 0.05.

Table 2. Average Feret diameter of the microparticles obtained for different thorium contents, expressed with a ± 2σ standard deviation.

Th content (mol.%)	Feret average diameter (nm)
0.5	1680 ± 200
1	1610 ± 260
2	1650 ± 220
5	1630 ± 240

II.2. Behavior under heating and characterization of calcined particles

II.2.1. TG analyses

In order to remove residual water and organics potentially present after the hydrothermal conversion step, and to monitor the chemical form of the oxide particles produced, raw samples were calcined either in reducing (Ar – 4% H_2) or in oxidizing (flowing air) atmosphere. The chemical transformations occurring upon heating were first monitored

by TG analyses. **Figure 5** presents the results obtained for x = 0.01, which are representative of the analyses performed for all the other compositions tested.

Under reducing atmosphere, the sample presented a continuous weight loss up to 1273 K, leading to a total Δm/m value of about -14%. This behavior is characteristic of hydrated oxides, and has been already reported for several chemical systems, including $(U,Ce)O_{2\pm\delta}$ or $(Th,Y)O_{2-\delta}$ [37, 38]. This weight loss was associated with the departure of residual water and organics, as well as to the reduction of $U_{0.99}Th_{0.01}O_{2+\delta}$ into stoichiometric $U_{0.99}Th_{0.01}O_{2.00}$. Although not fully complete at 1273 K, most of these processes occurred between 200 and 873 K. As such, the slight weight loss observed above 973 K only corresponds to the elimination of the last traces of amorphous carbon that are known to be particularly difficult to eliminate in the absence of oxygen [39].

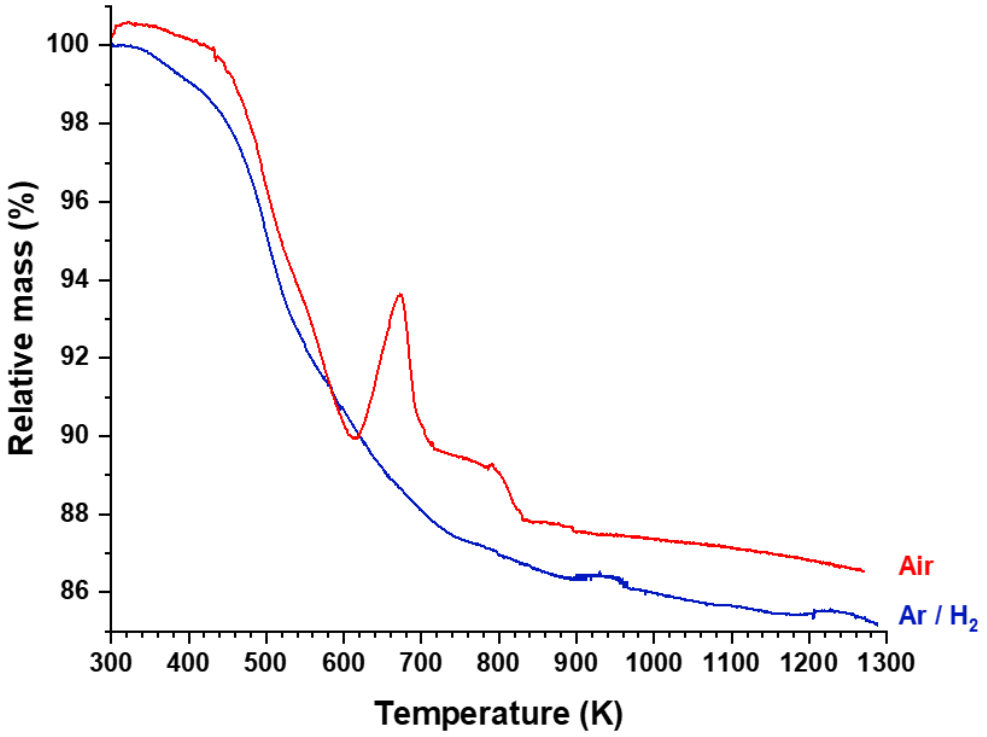

Figure 5. TG analyses of $U_{0.99}Th_{0.01}O_{2+\delta}.nH_2O$ performed in air (red) or under Ar-4% H_2 (blue).

Under oxidizing atmosphere (air), the behavior of the sample appeared to be much more complex, mainly due to redox reactions involving uranium. Indeed, while the TGA curve mostly followed the same trend than the one acquired under Ar-4% H_2 atmosphere up to around 623 K, a strong mass gain occurred at this temperature. This latter was assigned to the complete oxidation of U(IV) into U(VI), leading to the formation of a UO_3-like phase. A second mass variation was further observed at 823 K with a sudden weight loss corresponding to the partial reduction of uranium, and the subsequent formation of U_3O_8. In both cases, the

temperatures spotted agree well with those reported by several authors in the literature, especially when studying the decomposition of U(IV) oxalates or carbonates in air [40], or the incorporation of trivalent lanthanides into U_3O_8 through the thermal conversion of Ln-doped ammonium diuranate [41]. Above 873-973 K, the sample finally presented the similar residual weight loss observed in reducing atmosphere, and reached a final Δm/m value of about -13%. Overall, firing at 973 K or above appeared to be necessary under both atmospheres tested to ensure the elimination of the most important part of the volatile by-products coming from the wet-chemistry synthesis process.

II.2.2. PXRD

In order to specify the nature of the phases formed after heat treatment at high temperature either under reducing or oxidizing atmospheres, PXRD patterns were recorded for samples fired at 1273 K for 4 hours (**Figure 6**). Such a temperature was chosen in order to improve the crystallization state of the powders, and further facilitate Rietveld refinement of the data.

Under Ar-4% H_2 atmosphere, all the patterns collected confirmed the formation of single-phase $U_{1-x}Th_xO_{2+\delta}$ solid solutions, with only the XRD peaks of the fluorite-type structure observed. Thanks to the heat treatment at high temperature, the width of the XRD lines was significantly narrowed compared to raw samples, thus evidencing crystallite growth. This was confirmed by the Rietveld refinement of the data, which led to estimate the average crystallite size between 50 and 150 nm (**Table *3***), in good agreement with the data reported by Martinez *et al.* for comparable samples in the $(U,Ce)O_2$ system [37]. The unit cell parameters determined still remained below those expected from the linear variation between reference values, even if they stand above the data obtained from as-precipitated powders.

Table 3. Unit cell parameter and average crystallite sizes of the $U_{1-x}Th_xO_{2+\delta}$ samples obtained after heat treatment of raw particles at 1273 K under Ar-4% H_2 for 4 hours.

x	**0.01**	**0.02**	**0.05**	**0.10**	**0.30**
a (Å)	5.4504(5)	5.4443(6)	5.4601(8)	5.4700(4)	5.4902(6)
Crystallite size (nm)	80	160	108	50	82

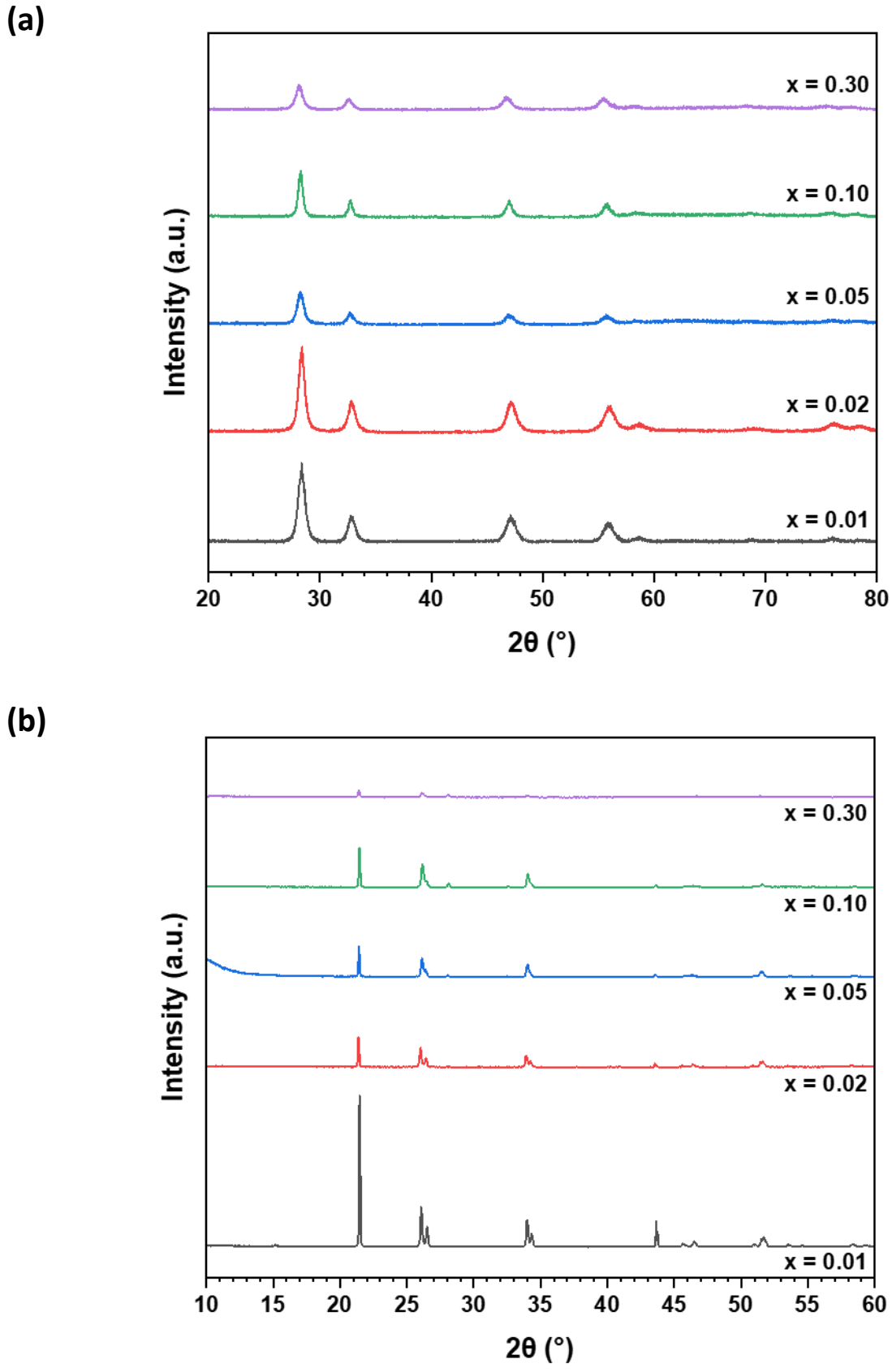

Figure 6. PXRD patterns of uranium-thorium oxide micro-particles obtained after heat treatment at 1273 K during 4 hours in Ar-4% H_2 (a) or in flowing air (b).

Under air, two distinct types of samples can be distinguished depending on the thorium incorporation rate (**Table 4**). Up to x = 0.02, the patterns only consisted of the PXRD lines of the orthorhombic structure of U_3O_8 [42], which is well-known to be the stable form of uranium oxides in air in this range of temperature. The unit cell parameters determined by Rietveld refinement showed a slight deviation from the values usually reported in the literature, indicating that, despite of its tetravalent oxidation state, thorium could be incorporated in limited amounts in the structure.

For thorium contents of 5 mol.% and above, additional PXRD lines characteristic of the fluorite-type structure of AnO_2 were also spotted on the patterns, particularly around 27° and 33°. The formation of a secondary product when increasing the thorium amount evidences the demixion of U- and Th-bearing phases, as the result of the different redox behavior of the two cations under air. Rietveld refinement of the PXRD data revealed that the mass fraction of the AnO_2 phase increased with the thorium amount, starting from 3 wt.% for x = 0.05 to around 20 wt.% for x = 0.30. Also, one must note that associated unit cell parameter remained systematically close to 5.51 Å, which corresponds to U-depleted oxides compared with the starting composition.

Table 4. Unit cell parameter of the MOx phases (with M = U+Th) obtained after heat treatment of raw particles at 1273 K under air for 4 hours.

Phase	**x**	**0.01**	**0.02**	**0.05**	**0.10**	**0.30**
MO_2	**a (Å)**	-	-	5.5127(9)	5.507(1)	5.5120(7)
	wt.%	0	0	3	7	21
M_3O_8	**a (Å)**	6.7335(2)	6.7373(1)	6.7639(6)	6.7582(3)	6.7662(2)
	b (Å)	11.9288(4)	11.9250(2)	11.8871(1)	11.8873(4)	11.8818(3)
	c (Å)	4.1486(1)	4.1511(2)	4.1586(4)	4.1560(1)	4.1623(1)
	wt.%	100	100	97	93	79

II.2.3. SEM observations

In order to evidence the modifications of micro-particles morphology under heat treatment, HT-ESEM observations were undertaken under the two atmospheres studied up to 1273 K. Although the spherical habit of the particles was conserved, their size varied all during the heat treatments (**Figure 7**).

Under reducing Ar-4%H_2 atmosphere, the particles were found to shrink continuously up to 773-873 K, as the direct consequence of the sample drying and the elimination of residual organics. Above this temperature, the averaged data obtained from the observation of three different particles became much more scattered, but seem to attest of a stabilization of the particle size up to 1223 K. Close to 1273 K, the beginning of an additional shrinkage step

was observed, which is probably related to the sintering of the particles, and/or to the growth of the elementary crystallites constituting the particles.

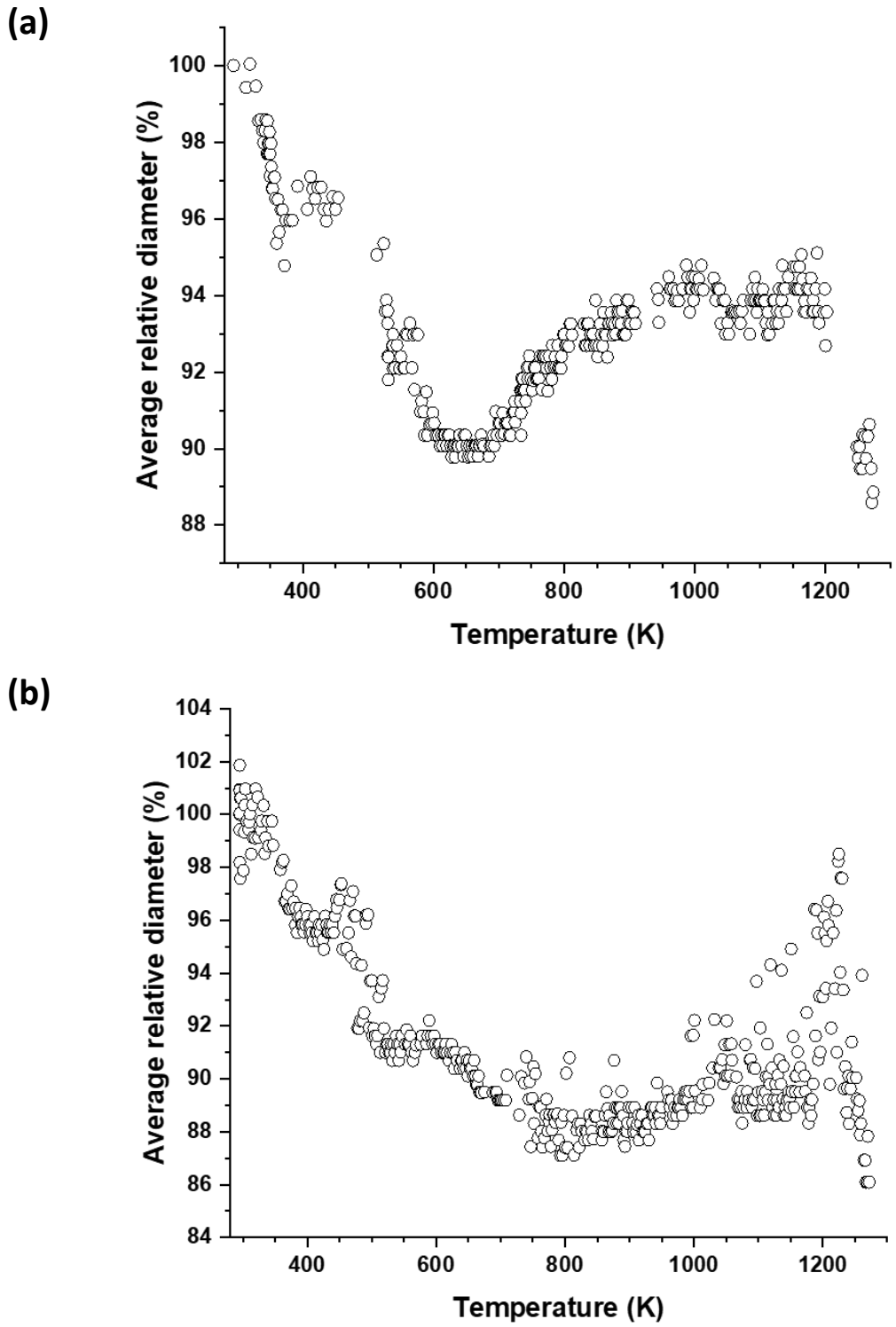

Figure 7. Variation of the average relative diameter of uranium-thorium oxide micro-particles (x = 0.05) determined by HT-ESEM observations under Ar - 4% H_2 (a) and in air (b).

Under air, the size variation evidenced several distinct steps, which can be directly related to the chemical transformations already suggested by thermogravimetric analysis. First, a slight swelling of the samples was noted from around 423 to 573 K, and could be probably correlated to the oxidation of U(IV) into U(VI), probably leading to a UO_3-like phase. Although this range of temperature appears lower than that observed in TGA, it remains consistent owing to the differences in the operating conditions of both experiments, mainly regarding the gas pressure and the amount of sample involved. The diameter of the particles was further found to shrink up to 673 K, before a second step of swelling associated to the reduction of the sample into Th-doped U_3O_8. The diameter then remained stable between 873 and 1173 K, before decreasing drastically above this latter temperature, probably due to sintering phenomena.

Additional SEM observations were then performed on samples fired at 973 K either in air or in Ar-4%H_2 (**Figure 8**). All the micrographs collected confirmed that the particles remained spherical with a homogenous size distribution. Also, no sign of sintering was detected at this temperature, which means that the formation of necks between the particles was avoided, which is a mandatory aspect to consider if one wants to analyze individual objects. However, some agglomerates can still be spotted on the pictures. They were already formed after the synthesis process, and could probably be eliminated by a simple sonication step.

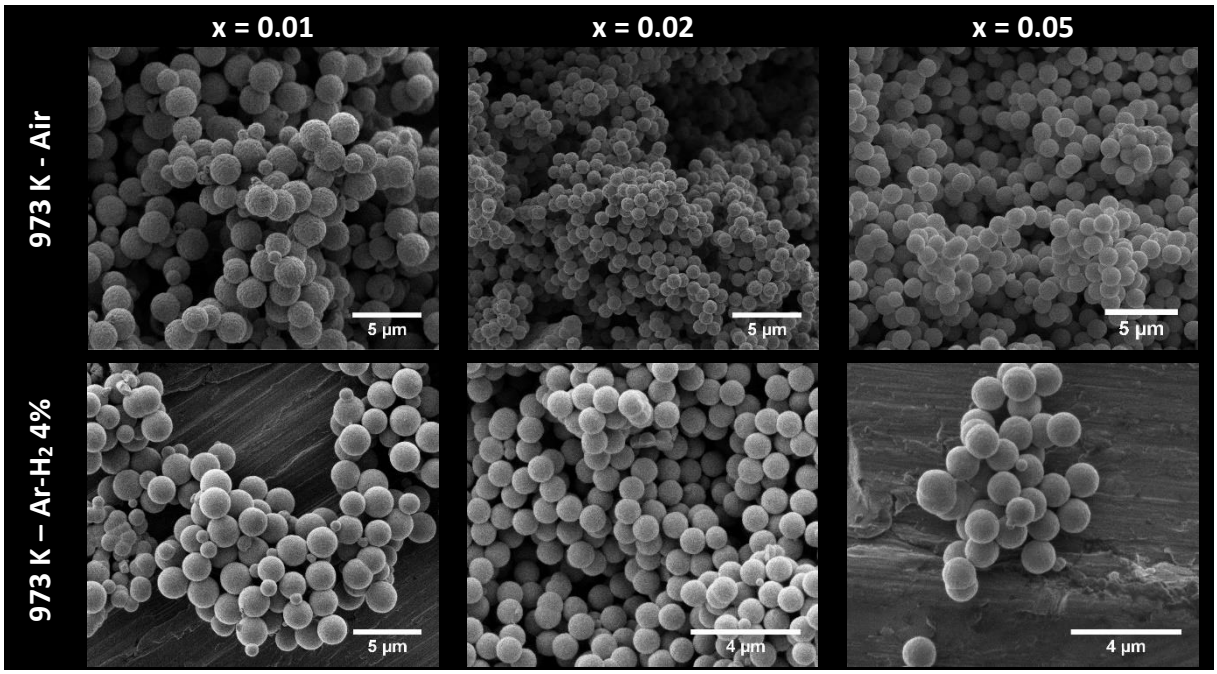

Figure 8. SEM observations of the uranium(IV)-thorium oxide particles obtained after heat treatment at T = 973 K during 4 hours under air or Ar - 4% H_2 atmosphere.

II.3. Evaluation of thorium distribution homogeneity within the samples

The homogeneity of the thorium distribution in the reference particulate material is one of the main requirements to achieve in order to guarantee the reliability of the isotopic measurements, for example by LG-SIMS analyses. Indeed, as these latter are generally conducted at the individual particle level, the doping rate in thorium must be controlled from the macroscopic to the sub-micrometric scale. In order to check the homogeneity of the thorium distribution in our sample, three different experimental methods were used to address these different scales.

The global chemical composition of the raw samples obtained after precipitation process was first determined by complete dissolution of the raw powders obtained after precipitation and subsequent PERALS measurements (**Table 5**), which allowed the quantification of alpha emitters with a good accuracy. For example Dacheux *et al.* noted a limit of detection of $1x10^{-9}$ M and $2x10^{-10}$ M for for ^{232}Th and ^{238}U, respectively, when using ALPHAEX as the extracting cocktail for a counting time of 3 days [43]. The Th/(U+Th) mole ratios obtained by PERALS measurements show a very good agreement between expected and experimental values. They confirm that the precipitation of both cations was quantitative in our operating conditions, whatever the amount of thorium incorporated up to 10 mol.%.

Table 5. Determination of the x = Th/(U+Th) mole ratio in the powdered $U_{1-x}Th_xO_{2+\delta}.nH_2O$ samples by complete dissolution followed by PERALS measurements, and by statistical EDS analyses. Uncertainties are expanded uncertainties with coverage factor of 2 ($\pm 2\sigma$).

x = Th/(U + Th) mole ratio		
Expected	***PERALS***	***EDS***
0.005	0.005 ± 0.002	0.005 ± 0.002
0.010	0.011 ± 0.002	0.010 ± 0.004
0.020	0.020 ± 0.002	0.021 ± 0.006
0.050	0.052 ± 0.003	0.051 ± 0.008

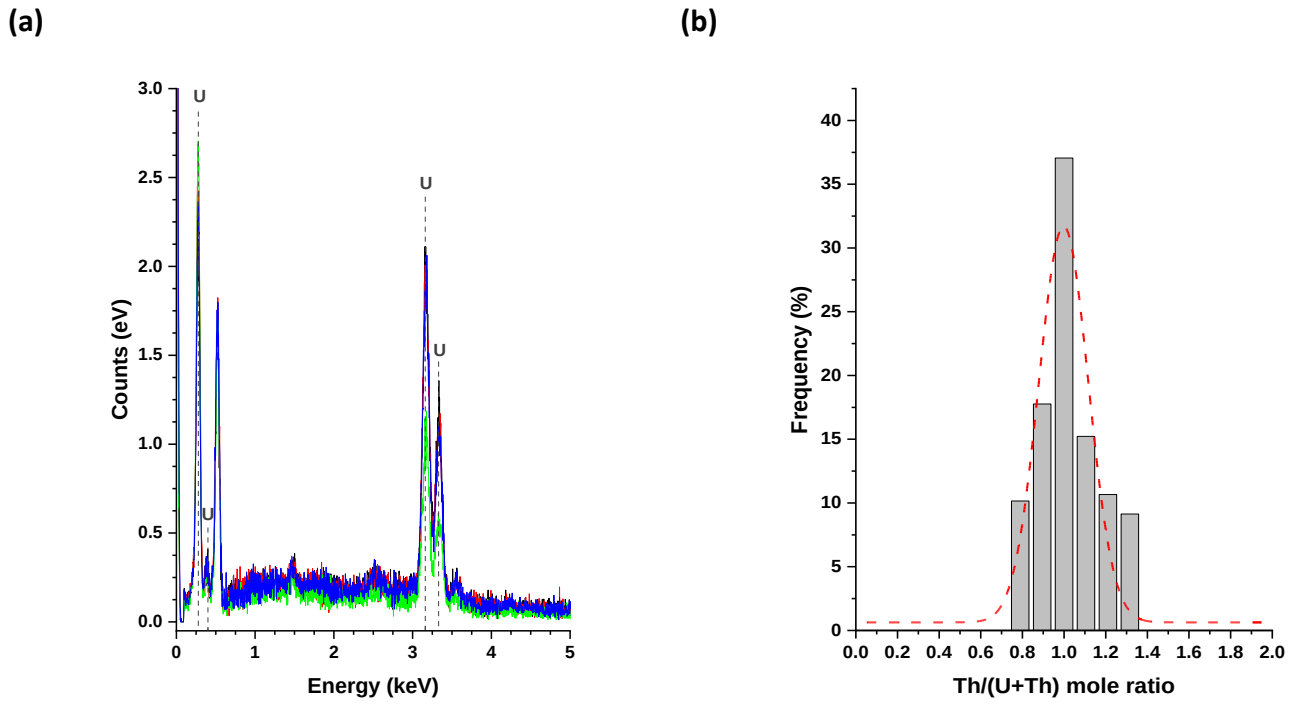

Figure 9. Example of four X-EDS spectra collected from the x = 0.01 sample (a), and statistical distribution of the Th/(U+Th) molar ratio (b).

The variability of the Th/(U+Th) mole ratio was further addressed at the global scale using statistical SEM/EDS analyses (**Figure 9**). Although only qualitative, visual examination of the superimposition of EDS spectra did not evidenced the formation of Th-enriched phases. Jointly with PXRD measurements, it allows to exclude the precipitation of distinct U- and Th-bearing phases, to the benefit of the formation of solid solutions. Moreover, the distribution of the Th/(U+Th) mole ratio measured by EDS analyses carried out on individual particles was found to be well fitted with a Gaussian law. The chemical composition is then expressed with a ±2σ confidence interval that encompasses 95% of the data points. The data reported in the **Table 5** confirm that the composition only presented a narrow distribution around the expected average value whatever the chemical composition considered in the raw samples. Nevertheless, owing to the volume probed during the analysis (approx. 1 μm^3) and that of the micro-particles (close to 2 μm^3), the small variations observed in the composition did not necessarily reflected the behavior of single objects. For example, the presence of multiple particles, or pores, under the electron beam can lead to level the final result.

In order to overcome this bias, LG-SIMS analyses were finally performed on single particles. In this case, we focused the study on a U_3O_8-type sample doped with 2 mol.% in thorium, obtained after heat treatment of the corresponding precursor in air at 973 K for 4 hours. Based on the results reported herein, such operating conditions correspond to single-phase and chemically stable sample, which is close to theoretical density. The measurements of the $^{232}Th^+/^{238}U^+$ isotopic ratio conducted on 28 distinct particles coming from the same batch show significant differences between particles, beyond expanded uncertainties of

individual measurements. However, these differences are relatively limited, with a relative external precision, expressed as twice the relative standard deviation over the 28 measurements (i.e. ~95% confidence interval), below 10%. (**Figure 10**). This reproducibility is regarded as satisfactory for age-dating analysis at the scale of the individual micrometric particles, owing to the very low amount (typically in the attogram range) of the daughter nuclide ^{230}Th in the particles.

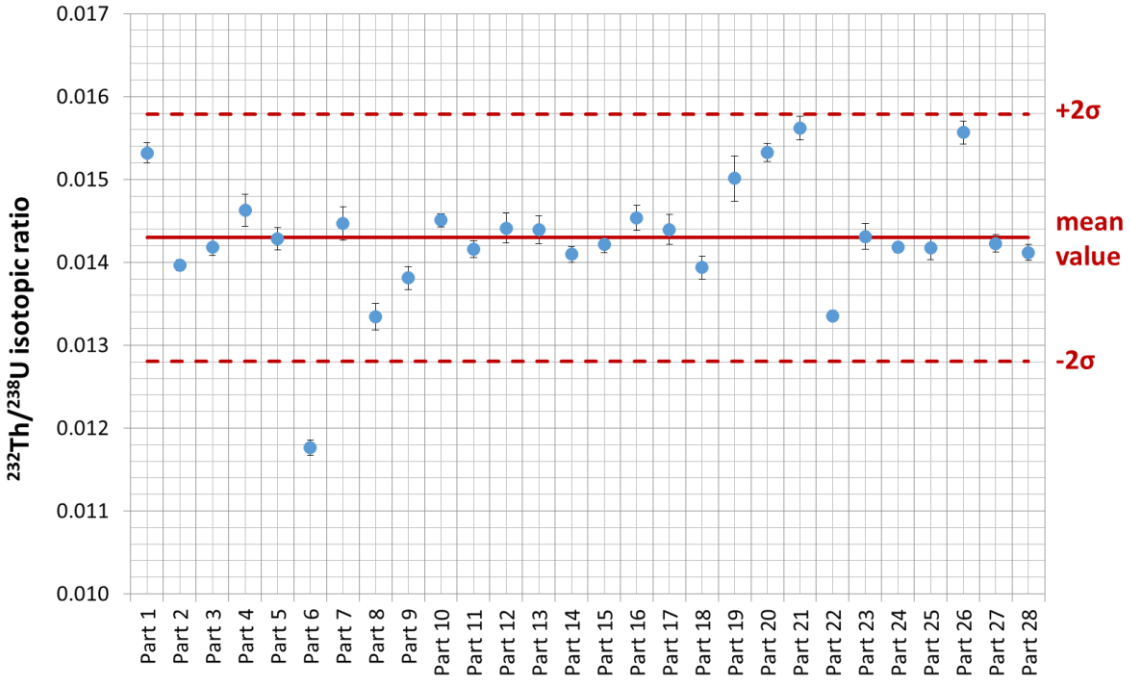

Figure 10. Distribution of the ^{232}Th/^{238}U isotopic ratio in 2 mol.% Th-doped U_3O_8, determined in 28 individual particles by LG-SIMS measurements.

The slight deviation of the average measured $^{232}Th^+/^{238}U^+$, (1.430 ± 0.075)×10^{-2}, from the expected value obtained by PERALS measurements, (2.0 ± 0.2)×10^{-2}, can be explained by the difference of the U and Th ionization yields within SIMS. To convert the $^{232}Th^+/^{238}U^+$ ion ratio into a ^{232}Th/^{238}U atomic ratio, the SIMS relative sensitivity factor (RSF) Th/U should be known. This factor can be calculated using the following equation:

$$RSF_{UTh} = \left(\frac{^{232}Th}{^{238}U}\right)_{reference} \Big/ \left(\frac{^{232}Th}{^{238}U}\right)_{measured} \quad (2.)$$

It should be noted that the calculation of the RSF requires a particulate material whose Th/U ratio is as accurately as possible known.

III. Discussion

III.1. Effect of thorium doping on raw particles structure/microstructure

Previous works allowed us to show that it was possible to synthesize morphology- and size-controlled uranium oxide microspheres from the hydrothermal conversion of U(IV) aspartate precursors [26]. With the aim to produce reference samples for the aging of uranium-bearing nuclear materials, the present results led to evaluate the effect of thorium doping on both the particles crystal structure, and microstructure. First, Rietveld refinement of PXRD analyses of the as-synthesized samples showed a quasi-linear variation of the unit cell parameter versus the thorium incorporation rate (**Figure 2**). As such, it evidences the formation of a solid solution, rather than the separate precipitation of UO_2 and ThO_2 oxides, despite the different temperatures reported in the literature for the hydrothermal conversion of Th- and U(IV)-aspartates [26, 44].

Nevertheless, one can note that the unit cell parameters determined in this study remain systematically below than those calculated from the linear variation between the reference unit cell parameters reported for UO_2 (5.4713 Å [35]) and ThO_2 (5.6032 Å [34]). Such a deviation probably originates from the partial oxidation of uranium(IV) into uranium(VI), either during the hydrothermal treatment step, or when storing the samples in air. Indeed, it is well known that the formation of hyper-stoichiometric UO_{2+x} oxides leads to a contraction of the unit cell, as the consequence of the decrease of the average ionic radius and the modification of the uranium coordination polyhedron, that evolves from a cube in $UO_{2.00}$ towards a cuboctahedron in U_4O_9 [45]. However, although some authors tried to link the unit cell parameter with the O/M stoichiometry, it remains difficult to estimate this latter in our case. Indeed, beyond the presence of thorium in the lattice, the nanosized character of our sample is likely to provoke an opposite effect tending to increase the unit cell parameter. Such a phenomenon was already highlighted in CeO_2 [46] and ThO_2 [47] samples, and was associated to the presence of species adsorbed onto the surface (that can be hydroxyl groups or organics) generating a tensile effect onto the lattice. On the basis of these results, and taking into consideration the fact that the formation of oxide phases during hydrothermal processes generally result from the aging of an hydroxide intermediate [33], we can propose the general formula of our samples to be written as $U_{1-x}Th_xO_{2+\delta}.nH_2O$, with a δ value that might evolve over time if no precaution is taken.

In the same time, the impact of thorium incorporation on the morphology of the spherical micro-particles precipitated was found to strongly depend on the doping rate. Up to 5 mol.%, it did not induce any modification of micro-particles size compared to pure uranium compounds reported in previous works [26]. Nevertheless, the progressive incorporation of thorium in the samples led to an enlargement of the PXRD peaks i.e. to smaller crystallites. As such, Th-doping slightly decreased the size of the elementary crystallites, but did not affect their assembly during hydrothermal treatment. Above 5 mol%. of thorium incorporation, SEM

observations revealed a drastic decrease of the microparticles size, which appeared to be typically between 50 and 250 nm in diameter. As the formation of microspheres was assigned to the self-assembly of elementary nanometric crystallites thanks to the adsorption of residual organic species [48], it is most likely that the incorporation of thorium in the samples modifies the surface chemistry of the crystallites, and precludes the formation of larger assemblies. Nevertheless, owing to the compositions targeted in the field of nuclear safeguards (typically lower than 1 mol.%), this does not appears as a limitation. Hence, the protocol proposed herein appears to be robust and not impacted significantly by the incorporation of thorium in the UO_{2+x} matrix.

III.2. Monitoring microparticles O/M stoichiometry

Beyond getting rid of the volatile species remaining from the wet-chemistry synthesis process, heating the raw micro-particles under controlled atmosphere was used in this work to monitor the final O/M stoichiometry (with M = U + Th), which can be of crucial importance if one wants to optimize the chemical durability of the samples under storage conditions. Hence, the raw micro-particles were calcined under both reductive (Ar - 4% H_2) and air atmosphere between 700 and 1000°C, and characterized from the structural and morphological point of views.

After heating under reducing atmosphere, the unit cell parameters determined from the PXRD data remained below those expected from the linear variation between UO_2 and ThO_2 reference values, even if they stand above the data obtained from as-precipitated powders. It is then most likely that the micro-particles were first reduced as stoichiometric $U_{1-x}Th_xO_{2.00}$ solid solutions during the heat treatment, as the thermodynamic stable form under our operating conditions ($pO_2 \sim 6\times10^{-29}$ atm.), then slightly re-oxidized when out of the furnace and stored under air. In this study, the final form of the material prepared under Ar-4%H_2 then has to be written as $U_{1-x}Th_xO_{2+\delta}$. Once again, the δ value certainly evolves over time owing to the reactivity of the powder, but evaluation of this effect was beyond the scope of this paper.

After heat treatment under air, the unit cell parameters determined by Rietveld refinement showed a slight deviation from the values usually reported in the literature for the well-known orthorhombic form of U_3O_8 [42]. In spite of its tetravalent oxidation state, thorium was then incorporated in limited amounts in the structure. While the incorporation of trivalent lanthanides into U_3O_8 was recently reported [41], this is the first time, to our knowledge, that thorium-doping has been clearly evidenced, as U-Th-O phase diagrams generally represent only U_3O_8 + M_4O_9 or U_3O_8 + $MO_{2+\delta}$ domains (with M = U + Th) [49]. Beyond the fundamental thermodynamics interest, this feature is also of particular importance in the field of particulate reference materials, since it allows to prepare single-phase and homogenous samples under the form of M_3O_8, which is expected to be the most chemically stable and durable one during storage in ambient conditions, either as loose powders or suspensions. Also, one must note that the XRD lines appeared to be significantly narrowed compared with that of the $U_{1-x}Th_xO_{2+\delta}$

solid solutions obtained under Ar-4% H_2, evidencing a drastic growth of the crystallites. This latter is consistent with the oxidation of U(IV) into a mixture of U(V) and U(VI), which is generally associated to an increase of the uranium diffusion coefficients [50].

Meanwhile, monitoring the evolution of the micro-particles morphology throughout heat treatments did not evidence drastic modification of their shape. Indeed, although their size was found to vary due to the elimination of volatile compounds (water and residual organics), densification processes and redox behavior of uranium, monodisperse spherical particles were always obtained after heating. Nevertheless, using high temperatures (typically around 1000°C) could lead to sintering phenomena, i.e. establishment of necks between adjacent particles. Based on these morphological evolutions, and considering the properties generally required for particulate reference materials (i.e. individual objects with controlled shape, close to 100% density, and chemically pure), the optimal temperature for firing our samples before use have been estimated to about 973 K. Indeed, TG analyses showed that such a preliminary heat treatment ensures the elimination of most of the residual water and organics, and also leads to the stabilization of the particle size whatever the calcination atmosphere considered.

III.3. Applicability of wet-chemistry processes for the preparation of highly homogenous samples

As one of the major requirements for the use of mixed uranium-thorium oxide micro-particles in the field of nuclear safeguards, the homogeneity of the cationic distribution in our samples was evaluated by means of different complementary techniques. Indeed, if the homogeneity of samples has been frequently addressed in the literature, it could concern very different size scales, leading the term 'homogeneous' sometimes senseless. As a matter of example, at the milli/micro-metric level, $(U,Pu)O_2$ MOx nuclear fuels prepared by dry chemistry processes could be depicted as homogeneous, provided the size of UO_2 agglomerates is small enough [51]. At the other end of the size-scale, compounds synthesized through wet-chemistry routes are generally tested by SEM- or TEM-EDS spectroscopy to confirm the homogeneity of the cationic distribution at the micro- or even nano-scale [37].

Herein, evaluating the chemical composition of the samples by different techniques pursued different goals. The first and more direct one was reached by the complete dissolution of the powders, and subsequent PERALS measurements, which confirmed the quantitative precipitation of the cations during the synthesis process. A statistical SEM-EDS analysis was then performed. This latter allowed us to probe approximately 1 μm^3 volumes, without any certainty of pointing individual particles. Hence, even if some bias might arise from probing areas containing different particles or voids, the results obtained systematically showed the simultaneous presence of uranium and thorium, with a small dispersion of the Th/(U+Th) mole ratio. As such, and despite of the difference in the conversion temperatures of thorium and uranium aspartates [26, 44], we can exclude the precipitation of the two cations in separate phases.

The more important point to be addressed still remained the cationic homogeneity at the particle scale, which was evaluated by LG-SIMS on 28 individual objects. Indeed, this point is of crucial importance in the frame of using the prepared micro-particles as reference materials, particularly to evaluate relative sensitivity factors during SIMS analyses [11]. Results obtained in this work showed a relatively low dispersion of the chemical composition around the average Th/(U+Th) mole ratio. Such a variability could appear surprising when using wet-chemistry processes, i.e. when starting from a homogeneous mixture of uranium and thorium in solution. It probably arises from the two-step hydrothermal conversion used herein. As such, the initial precipitate consists of an highly homogeneous U(IV)-Th(IV) aspartate, which is further decomposed by the joint action of pressure and temperature. The oxide micro-particles are then formed through the hydrolysis of U^{4+} and Th^{4+} cations. The differences in the hydrolysis constants [33, 52] and the saturation indexes at this stage then probably led to different precipitation kinetics that might provoke small variations in the composition of the particles, despite working under stirring. Nevertheless, the dispersion of the Th/(U+Th) ratio remained below 10%, which is considered as satisfactory for age-dating analysis through the ^{234}U - ^{230}Th radio-chronometer.

Conclusion

The synthesis of uranium-thorium mixed oxides particles was performed thanks to a wet chemistry route based on the hydrothermal conversion of U(IV)-Th(IV) aspartate precursors. Although solid solutions were obtained for all the chemical compositions tested in the $0.005 \leq Th/(U+Th) \leq 0.300$ range, as attested by PXRD, micro-particles with controlled morphology and size were only prepared up to 5 mol.% in thorium. In these conditions, the samples were found to consist of spherical aggregates composed of nanoscale crystallites, with a very narrow size distribution. Also, the size appeared to be independent of the thorium incorporation rate, and thus only controlled by the hydrodynamic conditions in the hydrothermal reactors. However, micro-particles still presented residual traces of water and organics coming from the synthesis process.

As a consequence, an additional heat treatment step was performed under various atmospheres, with the aim to get rid of impurities, to achieve complete densification of the micro-particles, and to monitor the chemical form of the final compounds. On the one hand, nearly stoichiometric $(U,Th)O_2$ dioxides were obtained under reducing $Ar\text{-}H_2$. On the other hand, heating under air led to the oxidation of uranium (IV) and to the formation of U_3O_8-based samples. Rietveld refinement of the PXRD data showed for the first time that Th(IV) remained incorporated in such samples up to 2 mol.%, while polyphase systems were obtained for higher Th-amounts. Although limited, the incorporation of thorium in U_3O_8 then allowed us to prepare mixed oxides micro-particles that should exhibit very high chemical stability during storage as a loose powder under ambient conditions.

Last, the homogeneity of the cations distributions in the samples was tested by various methods, allowing to address different size scales. As such, PERALS measurements and EDX

mappings led to confirm that the global chemical composition reached the targeted value, and that no segregation occurred between uranium and thorium during the precipitation process. More importantly, LG-SIMS analysis performed on nearly 30 individual microspheres showed significant but limited particle-to-particle variations. Indeed, relative external reproducibility (2σ) of the $^{232}Th^{+}/^{238}U^{+}$ ion ratios, remained below 10%, which is deemed satisfactory for use of these mixed oxide particles in the field of nuclear safeguards, as a reference particulate material for the datation of uranium particles thanks to the $^{230}Th/^{234}U$ radio-chronometer.

Acknowledgments

The authors would like to thank CEA for its continuous financial support, and for funding P. Asplanato PhD work.

References

[1] D.L. Donohue, *Anal Chem* **74**(1) (2002) 28a-35a.
[2] R. Zeisler, D.L. Donohue, *J Radioan Nucl Ch Ar* **194**(2) (1995) 229-235.
[3] S.P. LaMont, G. Hall, *J Radioanal Nucl Chem* **264**(2) (2005) 423-427.
[4] C.T. Nguyen, *Nucl Instrum Meth B* **229**(1) (2005) 103-110.
[5] Z. Varga, A. Nichol, M. Wallenius, K. Mayer, *Anal Chim Acta* **718** (2012) 25-31.
[6] Z. Varga, G. Suranyi, *Anal Chim Acta* **599**(1) (2007) 16-23.
[7] M. Wallenius, A. Morgenstern, C. Apostolidis, K. Mayer, *Anal Bioanal Chem* **374**(3) (2002) 379-384.
[8] Z. Varga, K. Mayer, C.E. Bonamici, A. Hubert, I. Hutcheon, W. Kinman, M. Kristo, F. Pointurier, K. Spencer, F. Stanley, R. Steiner, L. Tandon, R. Williams, *Appl Radiat Isotopes* **102** (2015) 81-86.
[9] F.E. Stanley, *J. Anal At Spectrom* **27**(11) (2012) 1821-1830.
[10] C. Szakal, D.S. Simons, J.D. Fassett, A.J. Fahey, *Analyst* **144**(14) (2019) 4219-4232.
[11] A.L. Faure, T. Dalger, *Anal Chem* **89**(12) (2017) 6663-6669.
[12] S. Richter, J. Truyens, C. Venchiarutti, Y. Aregbe, R. Middendorp, S. Neumeier, P. Kegler, M. Klinkenberg, M. Zoriy, G. Stadelmann, Z. Macsik, A. Koepf, M. Sturm, S. Konegger-Kappel, A. Venzin, L. Sangely, T. Tanpraphan, *J Radioanal Nucl Chem* (2022).
[13] E. Remy, S. Picart, S. Grandjean, T. Delahaye, N. Herlet, P. Allegri, O. Dugne, R. Podor, N. Clavier, P. Blanchart, A. Ayral, *J Eur Ceram Soc* **32**(12) (2012) 3199-3209.
[14] H. Daniels, S. Neumeier, A.A. Bukaemskiy, G. Modolo, D. Bosbach, *Prog Nucl Energ* **57** (2012) 106-110.
[15] A. Kumar, J. Radhakrishna, N. Kumar, R.V. Pai, J.V. Dehadrai, A.C. Deb, S.K. Mukerjee, *J Nucl Mater* **434**(1-3) (2013) 162-169.
[16] D. Hudry, C. Apostolidis, O. Walter, T. Gouder, E. Courtois, C. Kubel, D. Meyer, *Chem-Eur J* **19**(17) (2013) 5297-5305.
[17] R. Middendorp, M. Durr, D. Bosbach, *Procedia Chem* **21** (2016) 285-292.
[18] R. Middendorp, M. Durr, A. Knott, F. Pointurier, D.F. Sanchez, V. Samson, D. Grolimund, *Anal Chem* **89**(8) (2017) 4721-4728.
[19] P. Kegler, F. Pointurier, J. Rothe, K. Dardenne, T. Vitova, A. Beck, S. Hammerich, S. Potts, A.L. Faure, M. Klinkenberg, F. Kreft, I. Niemeyer, D. Bosbach, S. Neumeier, *Mrs Adv* **6**(4-5) (2021) 125-130.
[20] S. Neumeier, R. Middendorp, A. Knott, M. Durr, M. Klinkenberg, F. Pointurier, D.F. Sanchez, V.A. Samson, D. Grolimund, I. Niemeyer, D. Bosbach, *Mrs Adv* **3**(19) (2018) 1005-1012.

[21] G.I. Nkou Bouala, N. Clavier, R. Podor, J. Cambedouzou, A. Mesbah, H.P. Brau, J. Lechelle, N. Dacheux, *Crystengcomm* **16**(30) (2014) 6944-6954.
[22] J. Manaud, J. Maynadie, A. Mesbah, M.O.J.Y. Hunault, P.M. Martin, M. Zunino, D. Meyer, N. Dacheux, N. Clavier, *Inorg Chem* **59**(5) (2020) 3260-3273.
[23] R. Zhao, L. Wang, Z.F. Chai, W.Q. Shi, *Rsc Adv* **4**(94) (2014) 52209-52214.
[24] L. Wang, R. Zhao, X.W. Wang, L. Mei, L.Y. Yuan, S.A. Wang, Z.F. Chai, W.Q. Shi, *Crystengcomm* **16**(45) (2014) 10469-10475.
[25] N. Dacheux, V. Brandel, M. Genet, *New J Chem* **19**(10) (1995) 1029-1036.
[26] V. Trillaud, J. Maynadie, J. Manaud, J. Hidalgo, D. Meyer, R. Podor, N. Dacheux, N. Clavier, *Crystengcomm* **20** (2018) 7749-7760.
[27] C. Frontera, J. Rodriguez-Carvajal, *Physica B* **350**(1-3) (2004) E731-E733.
[28] P. Thompson, D.E. Cox, J.B. Hastings, *J Appl Crystallogr* **20** (1987) 79-83.
[29] C.A. Schneider, W.S. Rasband, K.W. Eliceiri, *Nature Methods* **9**(7) (2012) 671-675.
[30] G. Kauric, O. Walter, A. Beck, B. Schacherl, O.D. Blanco, J.F. Vigier, E. Zuleger, T. Vitova, K. Popa, *Mater Today Adv* **8** (2020).
[31] K. Popa, O. Walter, O.D. Blanco, A. Guiot, D. Bouexiere, J.Y. Colle, L. Martel, M. Naji, D. Manara, *Crystengcomm* **20**(32) (2018) 4614-4622.
[32] R.D. Shannon, *Acta Crystallogr A* **32**(Sep1) (1976) 751-767.
[33] D. Rai, A.R. Felmy, J.L. Ryan, *Inorg Chem* **29**(2) (1990) 260-264.
[34] V.K. Tripathi, R. Nagarajan, *Inorg Chem* **55**(24) (2016) 12798-12806.
[35] G. Leinders, T. Cardinaels, K. Binnemans, M. Verwerft, *J Nucl Mater* **459** (2015) 135-142.
[36] D. Hudry, J.C. Griveau, C. Apostolidis, O. Walter, E. Colineau, G. Rasmussen, D. Wang, V.S.K. Chakravadhaluna, E. Courtois, C. Kubel, D. Meyer, *Nano Res* **7**(1) (2014) 119-131.
[37] J. Martinez, N. Clavier, A. Mesbah, F. Audubert, X.F. Le Goff, N. Vigier, N. Dacheux, *J Nucl Mater* **462** (2015) 173-181.
[38] N. Clavier, Y. Cherkaski, J. Martinez, S. Costis, T. Cordara, F. Audubert, L. Brissonneau, N. Dacheux, *Chemphyschem* **18**(19) (2017) 2666-2674.
[39] J. Martinez, N. Clavier, T. Ducasse, A. Mesbah, F. Audubert, B. Corso, N. Vigier, N. Dacheux, *J Eur Ceram Soc* **35**(16) (2015) 4535-4546.
[40] L. Desfougeres, E. Welcomme, M. Ollivier, P.M. Martin, J. Hennuyer, M.O.J.Y. Hunault, R. Podor, N. Clavier, L. Favergeon, *Inorg Chem* **59**(12) (2020) 8589-8602.
[41] S.K. Potts, P. Kegler, G. Modolo, S. Hammerich, I. Niemeyer, D. Bosbach, S. Neumeier, *Mrs Adv* **7**(7-8) (2022) 128-133.
[42] B.O. Loopstra, *Acta Crystallogr* **17**(6) (1964) 651-&.
[43] N. Dacheux, J. Aupiais, O. Courson, C. Aubert, *Anal Chem* **72**(14) (2000) 3150-3157.
[44] N. Clavier, J. Maynadie, A. Mesbah, J. Hidalgo, R. Lauwerier, G.I. Nkou Bouala, S. Parres-Maynadie, D. Meyer, N. Dacheux, R. Podor, *J Nucl Mater* **487** (2017) 331-342.
[45] L. Desgranges, G. Badinozzi, D. Simeone, H.E. Fischer, *Inorg Chem* **50**(13) (2011) 6146-6151.
[46] D. Prieur, W. Bonani, K. Popa, O. Walter, K.W. Kriegsman, M.H. Engelhard, X.F. Guo, R. Eloirdi, T. Gouder, A. Beck, T. Vitova, A.C. Scheinost, K. Kvashnina, P. Martin, *Inorg Chem* **59**(8) (2020) 5760-5767.
[47] T.V. Plakhova, A.Y. Romanchuk, D.V. Likhosherstova, A.E. Baranchikov, P.V. Dorovatovskii, R.D. Svetogorov, T.B. Shatalova, T.B. Egorova, A.L. Trigub, K.O. Kvashnina, V.K. Ivanov, S.N. Kalmykov, *J Phys Chem C* **123**(37) (2019) 23167-23176.
[48] L. Wang, R. Zhao, C.Z. Wang, L.Y. Yuan, Z.J. Gu, C.L. Xiao, S.A. Wang, X.W. Wang, Y.L. Zhao, Z.F. Chai, W.Q. Shi, *Chem-Eur J* **20**(39) (2014) 12655-12662.
[49] J.W. McMurray, S.L. Voit, T.M. Besmann, *J Am Ceram Soc* **99**(6) (2016) 2197-2209.
[50] H. Matzke, *J Nucl Mater* **30**(1-2) (1969) 26-35.
[51] M. Le Guellec, F. Lebreton, L. Ramond, P. Martin, A. Ndiaye, T. Gervais, G. Bernard-Granger, *J Eur Ceram Soc* (2022).
[52] P.L. Zanonato, P. Di Bernardo, Z. Zhang, Y. Gong, G. Tian, J.K. Gibson, L. Rao, *Dalton T* **45**(32) (2016) 12763-12771.